Journal of Advanced Joining Processes 6 (2022) 100119

Contents lists available at ScienceDirect

Journal of Advanced Joining Processes

journal homepage: www.sciencedirect.com/journal/journal-of-advanced-joining-processes

Automatic detection and prediction of discontinuities in laser beam butt welding utilizing deep learning

Dominik Walther [a,1,*], Leander Schmidt [b,1], Klaus Schricker [b], Christina Junger [c], Jean Pierre Bergmann [b], Gunther Notni [c,e], Patrick Mäder [a,d]

[a] Technische Universität Ilmenau, Data-intensive Systems and Visualization Group (dAI.SY), Max-Planck-Ring 14, 98693 Ilmenau, Germany
[b] Technische Universität Ilmenau, Production Technology Group, Gustav-Kirchhoff-Platz 2, 98693 Ilmenau, Germany
[c] Technische Universität Ilmenau, Department of Quality Assurance and Industrial Image Processing, Gustav-Kirchhoff-Platz 2, 98693 Ilmenau, Germany
[d] Friedrich Schiller University, Faculty of Biological Sciences, Fürstengraben 1, 07743 Jena, Gemany
[e] Fraunhofer Institute IOF, Albert-Einstein-Str. 7, 07749 Jena, Germany

ARTICLE INFO

Keywords:
CNN
LSTM
Laser beam butt welding
Error detection
Error prediction
Weld discontinuities

ABSTRACT

Laser beam butt welding of thin sheets of high-alloy steel can be really challenging due to the formation of joint gaps, affecting weld seam quality. Industrial approaches rely on massive clamping systems to limit joint gap formation. However, those systems have to be adapted for each individually component geometry, making them very cost-intensive and leading to a limited flexibility. In contrast, jigless welding can be a high flexible alternative to substitute conventionally used clamping systems. Based on the collaboration of different actuators, motions systems or robots, the approach allows an almost free workpiece positioning. As a result, jigless welding gives the possibility for influencing the formation of the joint gap by realizing an active position control. However, the realization of an active position control requires an early and reliable error prediction to counteract the formation of joint gaps during laser beam welding. This paper proposes different approaches to predict the formation of joint gaps and gap induced weld discontinuities in terms of lack of fusion based on optical and tactile sensor data. Our approach achieves 97.4 % accuracy for video-based weld discontinuity detection and a mean absolute error of 0.02 mm to predict the formation of joint gaps based on tactile length measurements by using inductive probes.

Introduction

Laser beam welding is the technique of choice for a wide range of industrial tasks. As economic efficiency, resource efficiency and sustainability become more and more important, the requirements on reliability, reproducibility and weld seam quality are increasing. In this context, laser beam butt welding of thin sheets of high-alloy steel can be really challenging due to the formation of joint gaps, affecting process stability and weld seam quality (Nagel et al., 2017). By exceeding the maximum gap bridgeability of the laser beam, the influence of joint gaps can cause lack of fusion (Hsu et al., 1998). This can affect the mechanical-technological properties of the weld seam and the leak-proofness, ending up in rejection (Chen et al., 2014). The formation of joint gaps can be attributed to two local and time-dependent interacting effects. The first effect is dominated by the low thermal conductivity and high thermal expansion of high-alloy steels (Radaj, 1988). The absorbed laser radiation results in an increase of temperature, causing strain due to the thermal expansion of steels (Seang et al., 2013). As a result of the temperature-induced forces, the sheets can displace, causing a joint gap in the center of the seam (Simon et al., 2013). This effect interacts with the formation of thermal induced contraction during the cooling down and solidification of the weld seam, which also can contribute to joint gap formation (Dal and Fabbro, 2016; Seang et al., 2013). To limit this phenomenon, it is common practice to use clamping devices. However, by hindering the formation of joint gaps, the internal stress increases, which can end up in distortion of the specimen (Schenk, 2011). Furthermore, it is necessary to adapt clamping systems for each component geometry individually, making them very cost-intensive and limiting flexibility. To overcome these disadvantages, jigless welding offers a high flexible workpiece positioning due to the collaboration of

* Corresponding author.
E-mail address: dominik.walther@tu-ilmenau.de (D. Walther).
[1] These authors contributed equally to this work.

https://doi.org/10.1016/j.jajp.2022.100119
Received 13 April 2022; Received in revised form 15 June 2022; Accepted 15 June 2022
Available online 22 June 2022

different actuators, motion systems or robots. First approaches in arc welding demonstrate jigless and fixture-less welding by the collaboration of arc welding robots and material handling robots which take the place of jigs and fixtures (Bejlegaard et al., 2018; Högel, 2017; Kampker et al., 2017). As a result, it was possible to achieve a significant increase in productivity while reducing the times for changeover and costs for design, manufacturing and installation of jigs and fixtures (Bejlegaard et al., 2018). However, due to the differences in process control, welding speed and positioning accuracy, it is not possible to transfer these approaches to laser beam welding. Moreover, existing approaches are not designed for an active position control of the joint gap, despite a gap control offers significant benefits regarding process stability, defect formation and the formation of internal stress and distortion. The realization of an active position control requires a reliable detection of the joint gap during the welding process. In terms of quality assurance, it is also necessary to detect gap-induced weld seam defects (e.g. lack of fusion). In this context, the use of thermographic cameras (Nilsen, 2017; Srajbr et al., 2011) and inductive probes (Nagel et al., 2017; Simon et al., 2013) has proven to be suitable. To fulfill the requirements of a real-time position control, a further data processing requires fast and reliable error detection and prediction algorithms. Deep learning approaches like recurrent neural networks (RNN) (Baxter, 1995) and convolutional neural networks (CNN) (LeCun et al., 1999) have proven their real-time capabilities (Shi et al., 2020; Vater et al., 2020), but have not been implemented for the detection and prediction of joint gaps during laser beam welding so far.

Therefore, this paper presents different methods to detect and predict joint gaps and gap-induced weld seam discontinuities utilizing deep learning for an effective error prediction and classification. In total, 30 welds were performed and analyzed by optical and tactile sensor methods. Since data acquisition is time-consuming and expensive, an approach for a synthetic generation of data is introduced to overcome the limitations due to the low number of samples.

Materials and methods

As a follow-up study of (Schmidt et al., 2021), laser beam butt welding experiments were performed and characterized by using optical and tactile sensors. Afterwards, the data were processed by several deep learning algorithms to predict the formation of joint gaps and detect gap-induced weld discontinuities. This section will give a brief summary about the technical details as well as the evaluation methods proposed in this paper.

Technical details

Welding setup

The experiments were carried out for high-alloy steel sheets (material: AISI 304 / X5CrNi18-10 / 1.4301) with a thickness of 1.0 mm. The samples were cut to size by laser cutting with a length of 300 mm and a width of 50 mm. Fig. 1a depicts the experimental setup. The welding process was carried out in butt joint configuration. Sheet 1 was fixed in position by a clamping jaw with a holding force of 1.2 kN while sheet 2 was allowed to move freely in X-Y plane. The angular distortion in Z-direction of sheet 2 was limited by an air gap of 0.1 mm between clamping jaw and specimen. Sheet 2 was initially positioned with zero-gap towards sheet 1 which is why the resulting joint gap could be determined during welding. The rolling direction of the sheets was oriented in welding direction. The welding process was carried out by a Trumpf TruDisk 5000.75 disc laser at welding speeds of 1 m/min and 5 m/min. An overview of both considered welding parameters is given in Table 1. The laser beam power was determined depending the welding speed for achieving full penetration welds. The relative movement between laser beam and steel sheets was realized by a six-axis robot (Kuka KR60-HA) whereby the laser processing head was mounted to the robot. All welds were repeated 15 times for statistical reliability.

Since the formation of joints gaps affects the energy absorption of the laser beam and the position of the specimens, optical and tactile sensors were integrated in the experimental setup to determine qualitative information regarding the thermal radiation field and to obtain informa-

Table 1
Welding parameters.

Parameter	parameter set 1	parameter set 2
Welding speed	$1\frac{m}{min}$	$5\frac{m}{min}$
Resulting welding duration	20 s	4 s
Laser beam power	400 W	1000 W
Focal diameter	274 µm	
Wavelength	1030 µm	
Rayleigh length	2.38 mm	

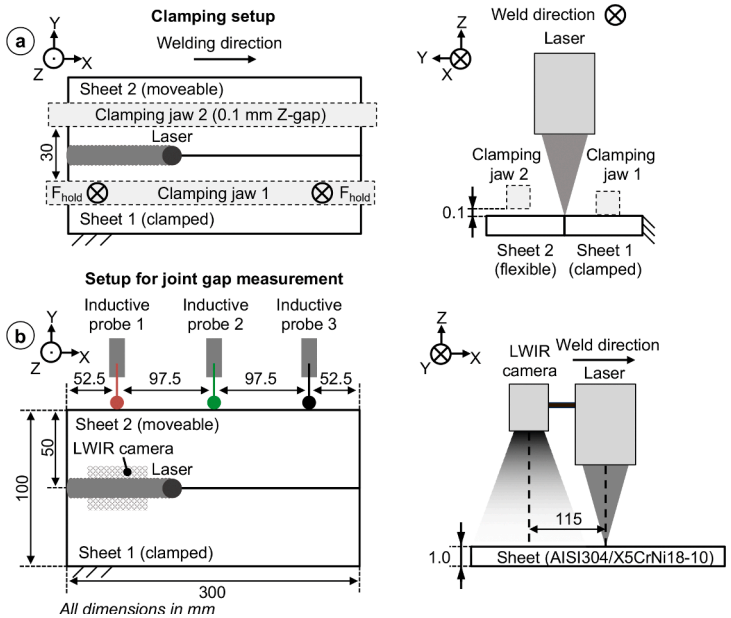

Fig. 1. Schematic of the experimental setup, separate illustration of: a) used clamping setup, b) used setup for joint gap measurement.

tion regarding the gap between both sheets during welding (see Fig. 1b). The change in Y-direction of sheet 2, moveable in X-Y plane, was measured by three inductive probes (Millimar P2010 M). The first one was positioned after 52.5 mm and with a constant distance of 97.5 mm between the following sensors. Changes in Y-direction provided information regarding the appearing joint gap. In contrast, changes in X-direction are of minor importance as the joint gap is decisive for the process termination. A measuring accuracy of 4 µm was reached within the measuring range of +/- 2 mm by using a measuring frequency of 1,000 Hz. The measured value of the inductive probes corresponds to the combined changes in position due to the strain field and the thermal expansion. The resulting gap change was simplistically calculated from the maximum values of these position changes. The relative movement of the laser beam by the robot allowed the detection of changes in Y-direction along the entire welding duration. A long-wave infrared camera (LWIR, InfraTec VarioCAM HD head 800) was used to determine gap-induced discontinuities based on irregularities of the thermal radiation field, which can be attributed to gap- and defect-induced changes in energy absorption and heat transfer. The spectral range of the camera is in the interval from 7.5 µm to 14.0 µm. The LWIR camera was mounted as near as possible on the processing head in trailing alignment, resulting in a distance between the laser beam axis and the LWIR camera axis of 115 mm. The measuring accuracy of the camera for determining absolute temperatures is +/- 1 K with a measuring range between 250 °C to 1,700 °C. A resolution of 1,024 px × 768 px and a recording frequency of 30 Hz was used.

Quality measure metric

The weld starts at the beginning of the sheet and should extend the entire specimen length of 300 mm as defect-free seam. A premature termination of the process can occur due to the joint gap resulting from the welding process, i.e. a discontinuity may occurred when the maximum gap bridgeability of the laser beam process has been exceeded. Considering that this article focuses on the prediction of the gap, the weld length ratio (WLR) was introduced to describe the ratio between achieved weld seam length L_{sound} to the entire specimen length L_{total} (see Fig. 2a and Eq. (1)).

Therefore, the WLR reaches the value 1 when the length of the sound weld extends over the entire specimen length or a value < 1 indicating a defective weld seam (see Fig. 2b). The dimensionless characteristic of WLR was preferable to use for machine learning. This procedure allowed the correlation between WLR and joint gap from the further acquired data in order to predict the opening of the gap. All specimens welded were inspected visually for discontinuities. The length of the sound weld seam L_{sound} was measured by photographs and used to calculate the WLR individually.

$$WLR = \frac{L_{sound}}{L_{total}}, WLR \in [0, 1] \tag{1}$$

The WLR distribution of welding parameter set 1 and welding parameter set 2 is illustrated in Fig. 3, indicating a increase in WLR for a rise in welding speed.

Evaluation methods

For the purpose of data analysis, the methods will be separated in two different tasks. First, methods to detect weld discontinuities and second, approaches to predict the joint gap formation and classify the weld quality. Previous attempts to detect weld discontinuities based data captured by a optical sensor employed Otsu threshold (Otsu, 1979), random forest (Breiman, 2001), multilayer perceptron (MLP) (Rumelhart et al., 1985) and convolutional neural network (CNN) (LeCun et al., 1999) for data analysis and classification. Thereby, Otsu threshold and random forest rely on predefined features, while MLP and CNN are approaches that automatically extract features for classifying a discontinuity. The subsection below briefly reviews each of these approaches.

Weld discontinuity classification

Otsu threshold. The Otsu threshold (Otsu, 1979) method searches for an optimal threshold value t^* to minimize intra-class and maximize inter-class variance for a given classification problem, such as weld discontinuity classification. Based on the changes in thermal radiation field induced by the formation of weld discontinuities, both classes (sound fusion and lack of fusion) should be separable by an optimal threshold t^*. Therefore, the Otsu threshold for two classes is calculated as follows:

$$\sigma_w^2(t^*) = \min_{t \in [1,254]} \omega_0(t)\sigma_0^2(t) + \omega_1(t)\sigma_1^2(t), \tag{2}$$

where the weights ω_0 and ω_1 refer to the probabilities of the classes separated by the threshold t; and σ_0 and σ_1 are the variances of the two classes e.g. defect-free seam and weld discontinuity. The algorithm searches for the best possible values of t to separate the two classes. To estimate the optimal Otsu threshold value t^*, the Python scikit-image processing library was used.

Random Forest. The random forest is a fast supervised approach to separate linear and non-linear features into classes. The method is a strong learner that combines multiple weak learning rule-based decision trees. A decision tree contains multiple branches that use conditions to split the tree into edges to differentiate between defect-free seam and weld discontinuity. The end node of a branch is called a decision leaf containing information to what class the data belongs (Breiman, 2001). A number of 25 decision trees was found suitable and employed throughout this study.

Multi-layer perceptron (MLP). A multi-layer perceptron (Rumelhart et al., 1985) is an artificial neural network. As the name implies, the MLP consists of multiple perceptrons ordered in a layer-wise manner. MLPs can be split up into three different types of layers. First an Input Layer which receives the input signal followed by n hidden and a final classification layer. The proposed MLP consists of three hidden layers

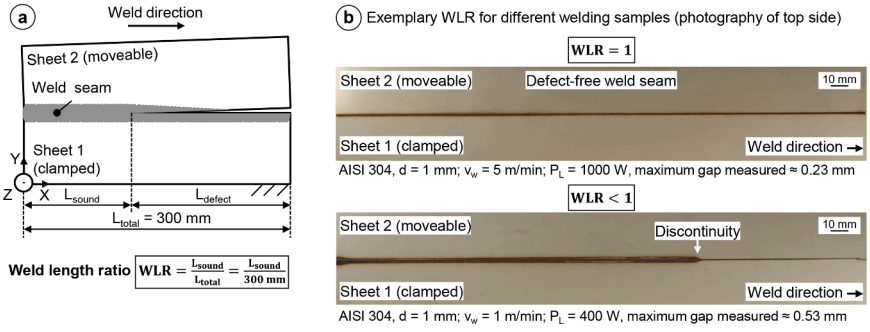

Fig. 2. Introduction of weld length ratio (WLR): a) specification of geometrical quantities during joint gap formation, b) photography of top side that shows the influence of the joint gap of weld discontinuities and correlating WLR.

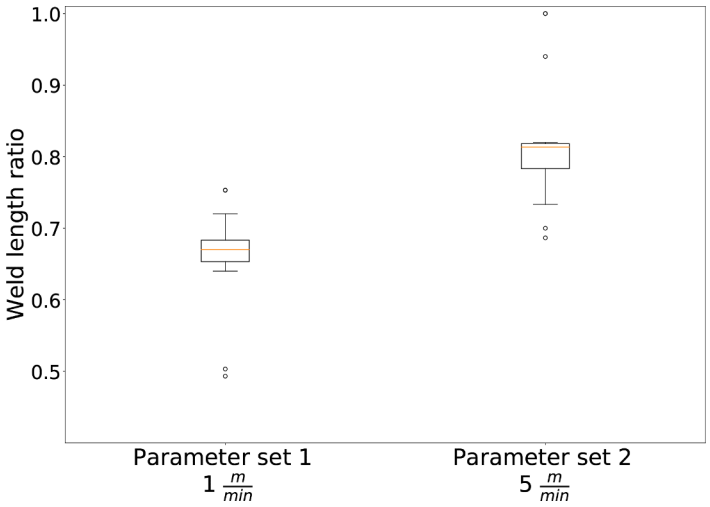

Fig. 3. WLR distribution of welding parameter set 1 and welding parameter set 2.

with 128 neurons each as depicted in Fig. 4. To prevent the model from over-fitting and improve the generalization, dropout layers with a dropout probability of 40 % and 20 % were added between the fully connected layers. Dropout (Srivastava et al., 2014) is a regularization technique that randomly sets a neurons activation to zero during training by a given probability. The neuron is not removed from the network, but disabled for the current training step. The processing pipeline for weld discontinuity classification based on LWIR camera recordings is depicted in Fig. 4. The LWIR camera recordings are cropped to focus on the region of interest. The MLP classifies whether the seam is defect-free or a discontinuity occurred.

Convolutional neural network (CNN). A convolutional neural network is a neural network architecture that efficiently learns representations in multi-dimensional data like images utilizing weight sharing. The network's fundamental operation is the convolution. By convolving input values, different types of features can be detected like edges in the early layers or more complex features in later layers. The proposed CNN architecture is depicted in Fig. 5 and consists of multiple convolutional layers followed by a batch-normalization layer. Batch-normalization is a common technique to reduce the networks covariate shift and accelerate the models training (Ioffe and Szegedy, 2015). Furthermore, a residual connection is added, helping the model to converge faster and reduce training time (He et al., 2016). The decision, whether a weld discontinuity occurred or not, is made by the last sigmoid activated fully-connected layer.

Prediction of gap formations and weld quality classification

A parallel and serial regression classifier based on an encoder-decoder LSTM (cp. Fig. 6) and an MLP are proposed within this study for predicting gap formation and classifying weld quality. The prediction of a future joint gap formation enables the possibility for realizing an active position control which is able to counteract the formation of discontinuities.

Recurrent neural networks (Baxter, 1995) like long short term memory (LSTM) (Hochreiter and Schmidhuber, 1997) are the prominent neural networks for sequence forecasting. LSTMs are capable of memorizing previous values in their history that is used when predicting future values. To do so, LSTMs take a sequence of length n as input to forecast the future course of the sequence. A specialized architectural pattern for time series forecasting consisting of two networks is called encoder-decoder architecture (Cho et al., 2014). The encoder-decoder setup consists of two independent LSTMs as depicted in Fig. 6, where a first LSTM encodes the input sequence and a second LSTM decodes and predicts future values of the sequence. This structure allows to process input sequences of any length and predict sequences of any other length.

Previous welding quality classification approaches were based solely on the measured gap at time step $t_{current}$ while the gap formation between $t_{current}$ until the end of the weld t_{end} was unknown.

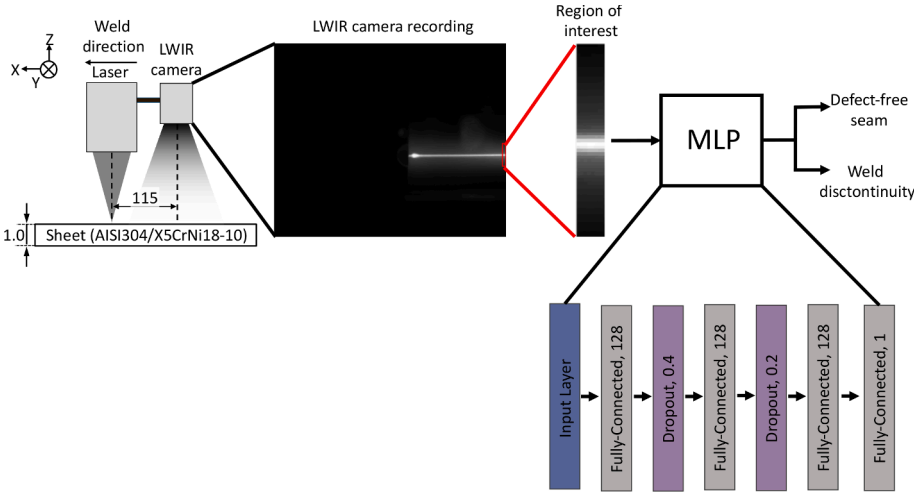

Fig. 4. Processing pipeline for weld discontinuity classification based on LWIR camera recordings with the proposed MLP architecture.

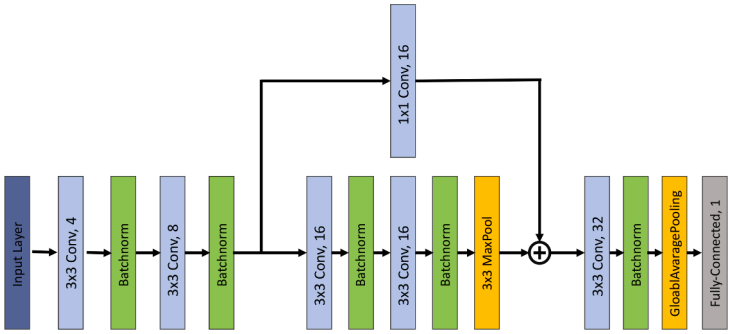

Fig. 5. Architecture of the proposed convolutional neural network for weld discontinuity detection.

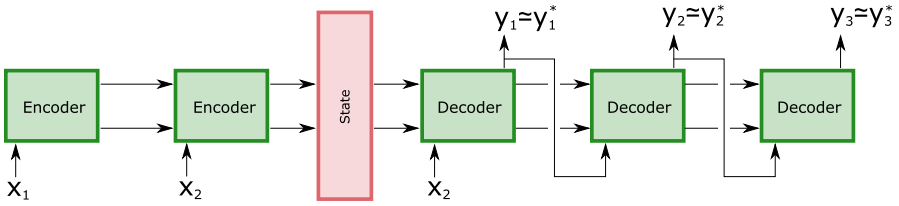

Fig. 6. Example of an encoder-decoder LSTM for sequence forecasting with x and y as measured and predicted joint gap formation, respectively.

This approach, where the classification is performed solely on the measured gap, will be referred to as parallel regression classifier (PRC). PRC consists of an encoder-decoder LSTM that predicts the joint gap formation and an MLP to classify the welding quality as depicted in Fig. 7. Here, the measured gap formation X is used as input for the encoder-decoder and the MLP. The result is a predicted gap formation Y_{reg} and a classification Y_{class} whereby both modules work in parallel.

However, since the encoder-decoder model can predict the further gap formation at time step $t_{current}$, it is possible to incorporate the prediction Y_{reg} into the classification. Therefore, a sequential regression classifier (SRC) as illustrated in Fig. 8 is proposed. The SRC combines an encoder-decoder LSTM and an MLP. However, in this solution both the predicted gap formation Y_{reg} and the input X are input to the classification MLP sequentially. Since the predicted joint gap formation Y_{reg} is also used for classification, the classification performance should be improved because the MLP yields not only the momentary but also the future joint gap formation. The classification is therefore not only more accurate but also earlier.

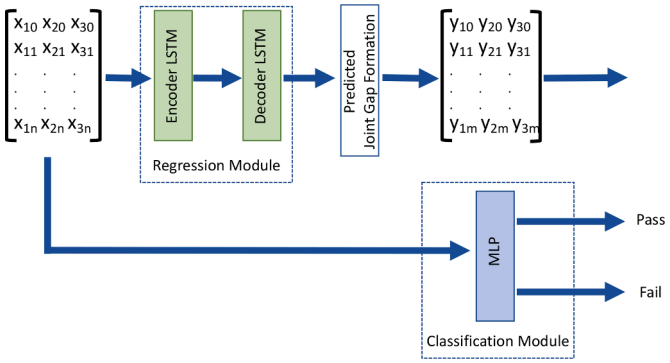

Fig. 7. Parallel setup for error prediction. Regression and classification module are disconnected from each other. The classification is based solely on recorded data.

Datasets

LWIR camera data

We extracted images from the LWIR camera recordings of each welding process resulting in 3,800 images showing sound fusion and lack of fusion. Each image was cropped to focus on the weld, removing unimportant segments of the images. Image segments that do not show a weld seam or the interaction zone of the laser and the sheets are not suitable for real-time analysis and removed from each image. Since the radiation field is recorded as a gray-scale image sequence, the pre-processed frame shape results in 59 px \times 9 px (height, width) with 550 frames showing lack of fusion and 3,250 frames showing sound fusion.

Since the thermal radiation field is affected by the energy absorption of the laser beam and heat transfer to surrounding material, the pixel values of each frame should change notably in the zone of lack of fusion. Therefore, different pixel features like mean, standard deviation, maximum, and minimum were extracted from each frame to receive a sequence of each feature over time. Each feature represents the visible changes regarding radiation field during the weld (Schmidt et al., 2021).

Inductive probe data

The inductive probes measure the formation of joint gaps for each weld at three positions (see Fig. 10) of the metal sheets. The recordings' number of data points varies depending on the welding speed of each parameter set, resulting in recordings with 20,000 data points for the first set and 4,000 data points for the second one. To adjust the different lengths of each welding parameter set, all samples after a weld discontinuity occurred were removed from each recording since these parts are unnecessary for an effective prediction of the joint gap. Furthermore, each shortened recording is down-sampled to a length of 650 data points.

Evaluation setup for error detection and prediction

Weld discontinuity detection based on LWIR camera recodings

Otsu threshold and the random forest approach are used with

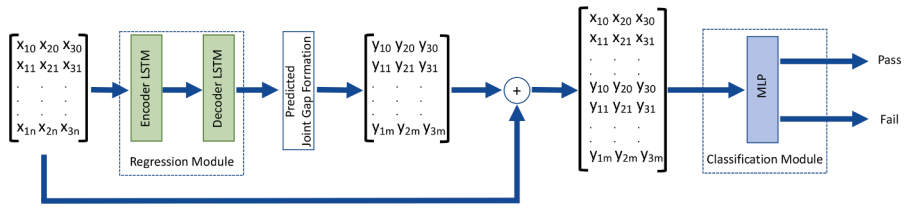

Fig. 8. Example of the serial setup for error prediction. Regression and classification module are connected with each other. The error prediction is based on recorded and predicted values from the regression module.

predefined features as baseline-classifiers to detect gap inducted weld discontinuities. Additionally, a multilayer perceptron representing a baseline for neural networks, and a convolutional network are trained to compare methods dependent on predefined feature extraction with techniques that incorporate feature extraction and classification. Leave-one-out cross-validation is used with 10 different sets to evaluate each of the introduced methods. The leave-on-out cross-validation uses 9 of the sets as training data and the remaining one as validation set. The method is repeated until each of the sets was used once during validation. Each cross-validation set contains frames from different video recordings to avoid similar files and ensure that each set differs. Since the number of frames showing defect-free seam is notably higher than frames showing weld discontinuities, only 550 defect-free frames are used to keep balance between the classes, resulting in a total of 55 frames for each class and cross-validation set. Each of the introduced methods in Section (Materials and Methods) is evaluated using the describe leave-one-out cross-validation technique. Based on the extracted LWIR camera features described in Section (Datasets), the changes of the thermal radiation field are received over time. To predict the formation of joint gaps, an encoder-decoder LSTM is trained to determine the relation between the radiation field and the joint gap formation.

Prediction of Gap formations based on inductive probe data

The prediction of joint gap formations is split into classification and regression tasks. The regression predicts geometrical changes of the flexible metal sheet, and the classification indicates whether the weld is sound or defective. Therefore, a total of 30 recordings with 15 recordings for each welding parameter set have been performed. Since the number of samples is not sufficient to train the regression module, additional synthetic samples that match the joint gap trends were generated by a non-linear least squares method. The non-linear least square method (Dennis and Welsch, 1978) is used to approximate different gap formations with a simple quadratic regression function as follows:

$$x(t) = c_2 \cdot t^2 + c_1 \cdot t + c_0 \tag{3}$$

with c_2, c_1, and c_0 as regression coefficients and x as function value at time step t. An example of a synthetic and a recorded welding process is illustrated in Fig. 9.

In total, 10 different cross-validation sets were created by randomly picking 5 recordings from each welding parameter set for validation and the remaining files for training, leading to 20 training and 10 validation samples for each of the cross-validation sets. For the synthetic sample generation, each of the training recordings was used to determine the best fitting coefficients c_2, c_1, and c_0 for inductive probe 1, 2, and 3, respectively. The mean and the standard deviation are calculated to receive a minimum and maximum range for each coefficient and lastly, a value based on the range of the coefficient is randomly picked. The resulting set of coefficients c_2, c_1, and c_0 is substituted into the regression function (cp. Eq. (3)) and one synthetic sample can be generated. The set of coefficients is picked 5000 times for each welding parameter set to generated a total of 10000 synthetic samples. This process is repeated for each cross-validation set to receive an equal number of training files for each set. An example of a synthetic sample and a recorded formation of the joint gap are illustrated in Fig. 9. The data from both settings described in Table 1 is used to train a regressor and a classifier to predict the formation of the joint gap and classify the welding quality. Since both welding parameter sets WLRs are notably different (cp. Fig. 3), this approach should be able to classify the weld quality if the WLR differs by a certain amount. The regression and classification module will be evaluated at different stages of the welding process ranging from 97 % to 37 % before the weld discontinuity occurs in order to analyze when a reliable prediction can be made.

Results and discussion

Characterization of joint gap formation

In order to demonstrate the effect of joint gaps on weld seam formation and correlating sensor data, Fig. 10 shows exemplary the formation of the weld seam by a photograph of the specimen top side in comparison to sensor data determined by LWIR camera and inductive probes for laser beam butt welding of 1 mm thick X5CrNi18-10 at a

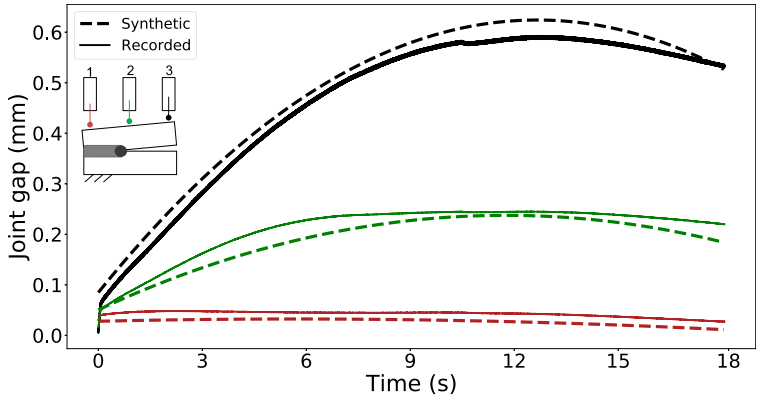

Fig. 9. Example of a synthetic and recorded formation of joint gaps for each inductive probe.

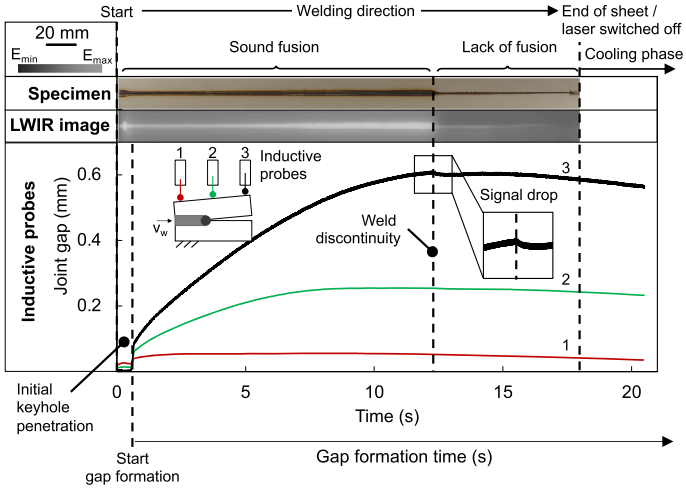

Fig. 10. Exemplary illustration of sensor data determined by LWIR camera and inductive probes in correlation to upper weld seam formation using 1 mm thick samples of X5CrNi18-10 at a welding speed of 1 m/min.

welding speed of 1 m/min.

The photograph of the specimen top side is characterized by two different zones of seam fusion. In this way, one zone of the seam shows a sound fusion, which extends from the process start to more than half of the total seam length. This is followed by the discontinuation of the weld seam, resulting in the formation of lack of fusion. By building the ratio between the weld seam length of sound fusion to the entire specimen length, the relating weld length ratio (WLR, see Section (Quality Measure Metric)) amounted to WLR = 0.68. In correlation to the LWIR recordings, this characteristic could be also found by analyzing the summation image of the thermal radiation field (technical details regarding the construction of the summation image can be found in Schmidt et al., 2021). In the zone of sound fusion, the seam can be identified by an area of increased thermal radiation. After the weld seam discontinued, the radiation signal drops significantly, representing the zone of lack of fusion. By analyzing the sensor data of the inductive probes, it is further possible to characterize the gap formation as function of time and local position. Immediately after exceeding the process begin, the signals of all three probes started to rise for a short time of about 0.7 s, which can be attributed to the initial piercing process of the keyhole. Subsequently, the signals fell back to zero line, before the relevant gap formation is initiated (starting time of gap formation). Depending on the local position of the probes, the course of the joint gap measured differs. While probe 1 is placed at the start of the weld seam and corresponding to a flat course of curve, the course of probe 3 is characterized by a much steeper rise in signal due to the positioning at the weld seam end. After reaching the joint gap maximum of about 0.59 mm, the signal of probe 3 also indicates the change in fusion by a signal drop, which can be attributed to a change in energy absorption by exceeding the maximum gap bridgeability of the laser beam. Following the signal drop, all three probe signals gradually decrease. This behavior continues after the laser beam is switched off and during cooling.

It can be stated that the LWIR camera recordings and inductive probe measurements can indicate the formation of weld discontinuities. Since the formation of the gap is decisive for weld discontinuities, the data of the inductive probes is used in the following to describe the underlying effects. Fig. 11 shows a combined view of all welds performed for the study to illustrate the relation between weld length ratio and maximum joint gap measured of each individual weld. It can be seen that the position of the probe had a significant effect on the maximum joint gap determined as discussed for the example given in Fig. 11. The comparison between parameter set 1 and parameter set 2 showed that a higher welding speed resulted in smaller maximum gap dimensions, especially salient for probe 3 positioned close to the end of the sheet. The increased

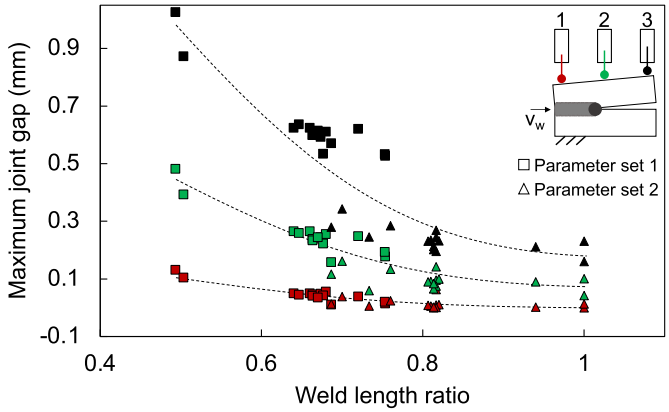

Fig. 11. Relation between measured maximum joint gap and weld length ratio. The image shows both welding conditions, i.e. parameter set 1 (represented by: □) with a welding speed of 1 m/min and parameter set 2 (depicted by: △) with a welding speed of 5 m/min, and the different positions of probe 1 (red), 2 (green), and 3 (black).

welding speed led to a reduction of laser beam power deposited in the material resulting in a narrower temperature field, a decreased weld seam width and thus reduced strain explaining the effect on gap width. This behavior was accompanied by larger ratios of WLR, i.e. the length of the sound weld was increased for a reduced maximum gap width measured. The overlapping in the data between probe 1 and 2 for both parameter sets in the range of WLR 0.7–0.8 support the presence of a possible relationship. However, the data points scatter around any comparison line which is why it is uncertain whether the maximum gap can actually provide a reliable and generally valid statement regarding the occurrence of gap-induced weld seam discontinuities. Further considerations of different welds and varying WLR followed for this reason.

Fig. 12 shows the time-dependent joint gap at probe positions 1–3 for three values of WLR: 0.51, 0.69 and 1.0. The welds for a WLR of 0.51 and 0.69 were obtained at a welding speed of 1 m/min (parameter set 1) and for WLR of 1.0 at 5 m/min (parameter set 2). It was confirmed by the temporal progress of the joint gap that smaller WLRs were accompanied by larger gap dimensions and that the gap increased in all cases from position of probe 1 to probe 3 and is decreasing after a certain time due to the complex thermo-mechanical system based on the interactions between material, thermal expansion and contraction of the weld. It is noticeable in the top view of the specimens that the edges of the sheet

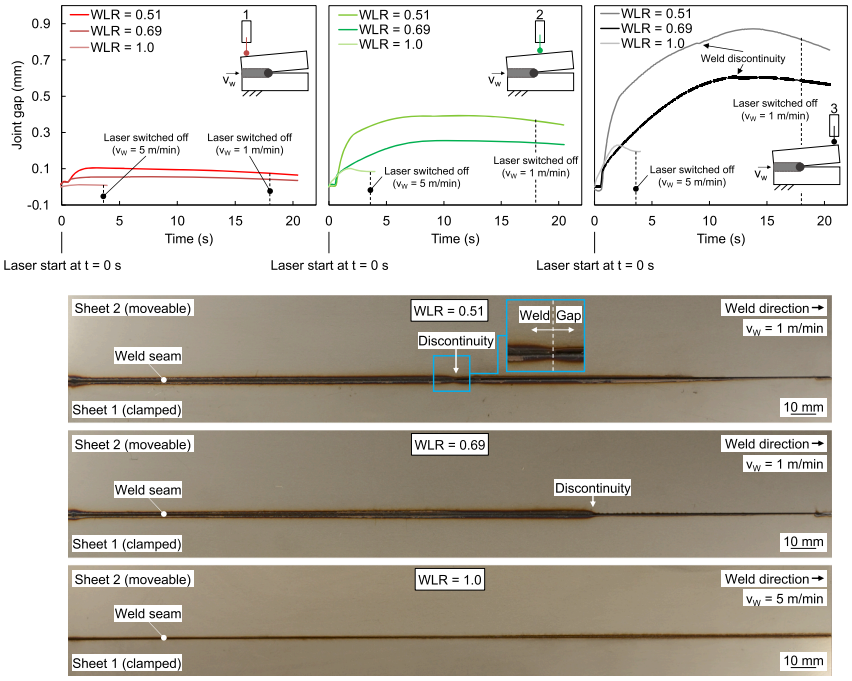

Fig. 12. Time-dependent joint gap at probe positions 1–3 for three different weld length ratios and images of each respective weld seam.

may be heated and partially melted even after the weld discontinuity occurred with both sheets separated by a gap (see detailed image at WLR = 0.51). The ongoing heat input resulted in an increased joint gap after the weld was discontinued which can be seen clearly for probe 3 where the maximum gap value was reached after approx. 14 s while the weld was interrupted after approx. 9 s. In contrast, an interruption of the weld occurred for a WLR of 0.69 after approx. 13 s at the corresponding maximum gap of probe 3. Comparing the curves of WLR 0.51 and 0.69 with WLR 1.0, it can be seen that the initial keyhole penetration is hardly detectable and the gap size increases significantly faster. At the same time, a complete weld over 300 mm is achieved. The gap reached its maximum after approx. 2 s, i.e. after a slightly longer time than it took to weld half the sheet length. It can be seen that the gap started to decrease afterwards which is noticeable throughout the gap values in probe 1–3. The main reason for this behavior can be seen as growing influence of constriction with increasing weld length. This illustrated that the process parameters affected the resulting gap significantly. However, a significant difference in the gap formation can be observed even under comparable experimental conditions as seen for WLR 0.51 and 0.69. This is due to the change in specific power deposition, for example when less volume is melted, the emerging weld seam geometry and the contraction during solidification and cooling in addition to the thermal-mechanical history of the sheet. It should be noted that the friction conditions between sheet and clamping jaw 2 (see Fig. 1 in Section (Welding Setup)) may affect the gap formation as well, e.g. if a bending occurs and may hinders the movement of sheet 2. The measurement of each individual joint gap over time ensured to cover its interaction with the resulting seam length correctly.

In terms of realizing a real-time capable position control which is able to counteract the formation of weld discontinuities (e.g. by clamping devices with actuators for controlling the gap based on mechanical forces), the formation of joint gaps and gap induced weld discontinuities must be predicted. Since the joint gap formation reflects the relevant events during welding and includes the effect of relevant influencing parameters in a time-dependent manner, it can be utilized for prediction. Due to the fact that the maximum joint gap is not a meaningful criterion for the weld discontinuity and since the sensor signals change significantly after initiation of a weld defect, the use of conventional data processing is not effective. Therefore, the following sections investigate different approaches for sensor data processing to realize an early and reliable detection of weld discontinuities and prediction of joint gap formations.

Weld discontinuity detection based on LWIR camera recodings

Four approaches were introduced to detect gap induced weld discontinuities based on LWIR camera recordings. Threshold detection and the random forest classifier scored the worst across all approaches. As shown in Fig. 13, both methods are capable of high accuracy values but also performed notably worse for some cross-validation sets. The worse performance mainly occurs when a set of features differs between training and validation data. With an average accuracy of 79.6 %, the threshold detection performed worse than the random forest classifier with an average accuracy of 81.6 %. Compared to traditional methods, both neural networks show an improved performance. The convolutional neural network performed best across all implemented methods and detected most frames correctly across all cross-validation sets. The CNN achieves an average accuracy of 97.4 % and performs slightly better than the MLP with detection accuracy of 96.2 %. All of the investigated methods are capable to detect weld discontinuities based on LWIR camera recordings. However, the results indicate that methods which rely on predefined features could miss weld discontinuities when the feature set does not contain sufficient information to differentiate between sound and lack of fusion. Furthermore the recorded changes of the thermal radiation field over time were used to predict the further formation of joint gaps with an encoder-decoder LSTM model. However, the model is not able to predict the formation of joint gaps based on the radiation fields changes. This indicates that a direct relation between joint gap and the thermal radiation field cannot be derived by the model.

Prediction of gap formations based on inductive probe data

The encoder-decoder LSTM is able to predict the formation of joint gaps based on the inductive probes' recordings. The mean absolute error (MAE) between the recorded and predicted joint gap formation is depicted in Fig. 14. Since probe 3 measures a much steeper signal rise

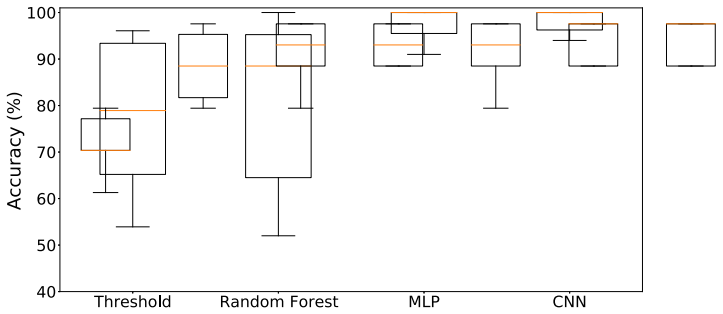

Fig. 13. Accuracy achieved by the presented approaches for weld discontinuity detection based on LWIR camera recordings. Shown is the median value (orange) with upper and lower quantile for the 10-fold cross validation. (For interpretation of the references to color in this figure legend, the reader is referred to the web version of this article.)

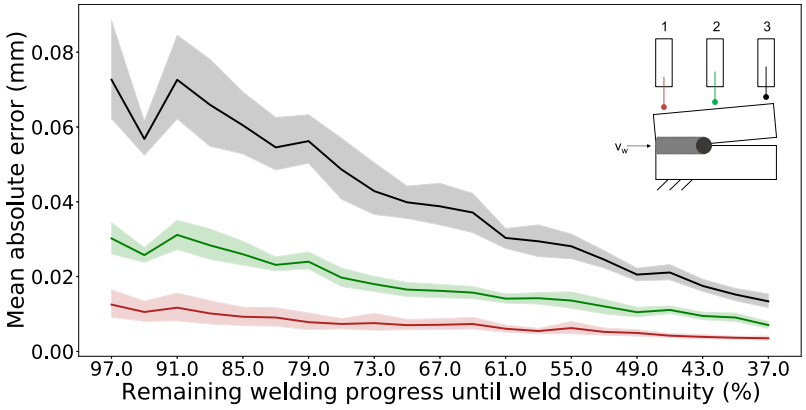

Fig. 14. Mean absolute error of the regression module at different welding stages for each inductive probe.

than probe 1 and 2 (cp. Fig. 10), it is expected that the MAE is higher compared to the other probes. Especially in early stages of the weld, the average MAE and standard deviation are notably higher compared to later stages, when more information about the gap formation is measured. The MAE between measured and predicted joint gap constantly decreases and the model's prediction becomes more precise.

The same trend can be seen, when comparing the classification capabilities of the PRC and SRC. As shown in Fig. 15, both approaches perform similar in early stages of the welding progress with a high standard deviation across the different cross-validation sets. At around 73 % before the weld discontinuity occurs, an increasing accuracy for the SRC, achieving better results than the PRC can be observed. In addition, a permanently decreasing standard deviation for the SRC is showing, which is not the case for the PRC. The regression module does not only help to classify the weld quality earlier, but also improves the classification accuracy of the MLP.

An example of a predicted joint gap formation is depicted in Fig. 16. In this case, 2.2 s of joint gap formation are measured by the inductive probes and about 9 s are predicted by the encoder-decoder LSTM. The predicted joint gap exactly matches the measured gap in the beginning, but deviates increasingly as the prediction progresses (cp. Fig. 16 third probe).

Since the regression module is able to predict the joint gap formation precisely, this approach can be suitable to enable an active position control to counteract the gap formation. Therefore, the regression module enables the possibility to counteract the gap formation not solely based on the current gap formation, but can be improved since the further gap formation is also known.

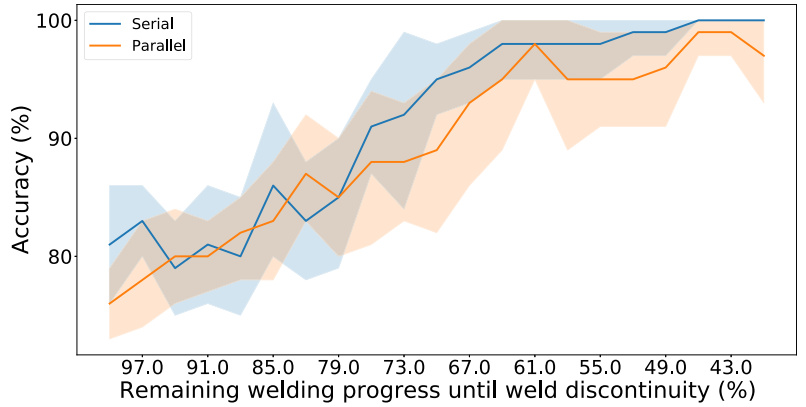

Fig. 15. Comparison of parallel (orange) and serial (blue) approach for weld quality classification at different welding stages. (For interpretation of the references to color in this figure legend, the reader is referred to the web version of this article.)

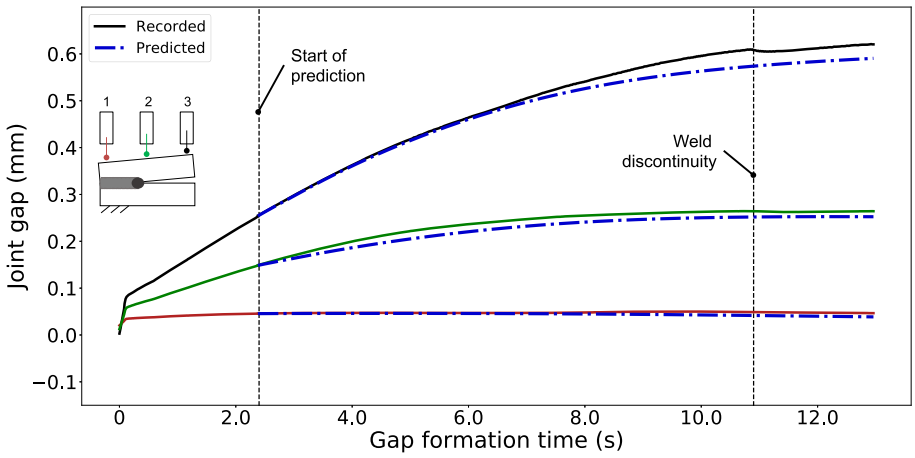

Fig. 16. Example of a predicted gap formation compared to measured joint gap for each inductive probe.

To investigate the importance of each probe for the classification module, different sensor combinations were used to classify the weld quality. As illustrated in Fig. 17, probe 1 contains the least information about the weld quality. Probes placed at the middle and the end of the sheet give the best indication about the quality. The performance of the classification module further improves when more than one probe is applied and a combination of probe 2 and 3 performed best. Comparing a combination of probe 1/2 and probe 1/3, the classification performance is better when the joint gap prediction of probe 2 is included. Therefore, it can be argued that probe 2 has the most impact on the weld classification and the models performance improves, when probe 2 is applied.

Transferability and application scenarios for laser beam welding

A novel methodological approach for describing and predicting the joint gap induced weld discontinuity was presented and successfully demonstrated its capabilities based on deep learning for different sensor signals and welding parameters. The weld discontinuity is based on the time-dependent formation of the joint gap that depends on a complex thermo-mechanical system affected by materials, joint configuration, process parameters and the clamping situation. The efforts regarding the transferability and applicability will be discussed based on three examples in the following.

- Example I – change of material: A change of the material would affect, among others, the thermal conductivity, the melting interval and the thermal expansion coefficient would change the temperature distribution, the weld seam geometry and the resulting stresses. However, since the physical relationships of joint gap formation are comparable, the developed methodology can be applied.
- Example II – changes in process parameters: A change in process parameters, e.g. focal diameter, laser wavelength or welding speed, would affect the resulting temperature distribution due to temporal and spatial energy input. Gap formation would be affected due to the interaction with the chosen material. As discussed for changes of the material, however, the relationships leading to gap formation would still remain valid, i.e. the applicability of the methodology developed is given. Hereby, the fundamental flexibility of the method has been shown by using two welding speeds based on parameter set 1 and parameter set 2 during the study presented in the paper. However, since the recorded gap formation would be notably different when the process parameters change during the weld, the deep learning models have to be retrained to learn the new gap formation behavior. It therefore can be assumed that the changes, which affect the gap formation over time, can still be handled by the deep learning model.
- Example III – change of joint configuration: A change of the joint configuration or joining geometry can have different effects. If the transfer is considered from a butt joint to a lap joint for comparable sheet thicknesses, the joining gap results primarily in the z-direction instead of in the x- or y-direction. The progress of the sheet displacement over time (Danielewski and Skrzypczyk, 2020) leading to the joint gap seems to be comparable to the butt joint, i.e. the methodical approach can be assumed to be applicable. The detection of false friends affected by the gap (Heller et al., 2015; Mrna and Hornik, 2016) could thus be addressed, for example. In case of transferring the method, for example, to very thick sheets with distinct distortion in different spatial directions, the presented procedure will reach its limits, since the gaps will form significantly

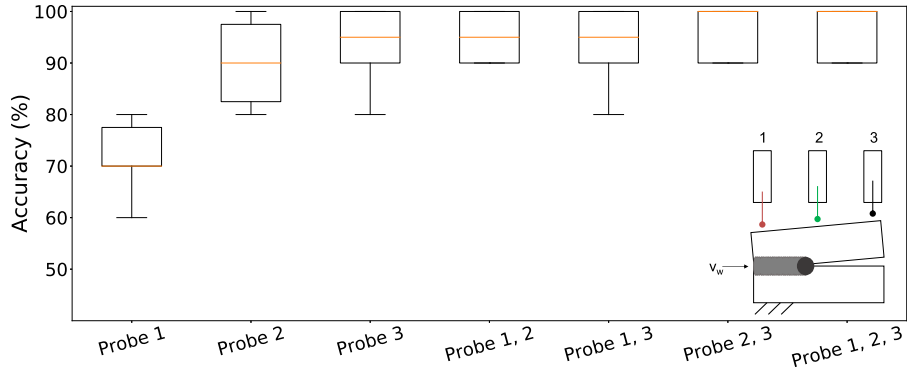

Fig. 17. Influence of different sensor combinations for weld quality classification.

different and additional factors could influence the weld discontinuity.

We demonstrated that the approach can be transferred to other scenarios for laser beam welding, by retraining on scenario specific data. Therefore, new datasets must be generated by recording additional welds. It is also conceivable to utilize the prediction of the joint gap for controlling welding processes, where the manipulation is not performed via the laser beam process, e.g. by adjusting the beam power, but via clamping devices equipped with actuators. Future work will address this group of issues in particular.

Conclusion and future work

This investigation focused on the detection and prediction of joint gap induced weld seam discontinuities for welding thin sheets of high-alloy steel in butt joint configuration. By optical and tactile measurements, it was shown, that the formation of joint gaps increased with a rise in welding time. After reaching the joint gap maximum, the formation of lack of fusion was observed, which can be attributed to a change in energy absorption by exceeding the maximum gap bridgeability of the laser beam. The change in weld seam fusion was reflected in a signal drop of both sensor systems, appearing only after defect initiation. Since the realization of a real-time capable position control requires an early and reliable detection and prediction of the joint gap and gap induced weld seam discontinuities, different methods for a processing of optical and tactile sensor data were developed and evaluated. In total, four different methods for processing thermal images recorded by LWIR camera were tested, exposing benefits in performance of deep learning methods with automatic feature extraction compared to traditional methods. Relating to this, the proposed CNN achieved 97.4 % accuracy on average for the 10-fold leave-one-out cross-validation to detect gap induced weld discontinuities. Furthermore, parallel and serial regression classifier to predict the formation of joint gaps and classify the welding process based on tactile sensor data of inductive probes were introduced and compared. Despite that it was possible to distinguish the welding process regarding the weld quality by using both methods, the serial regression classifier performed more precisely and could detect the phase of defect formation at earlier stages. The possibility of the precise gap and defect prediction will enable the future development of suitable countermeasures to control the gap formation by an active position control with the aim of eliminating weld discontinuities.

Acknowledgment

The Project ‘Engineering for Smart Manufacturing (E4SM) Engineering of machine learning-based assistance systems for data-intensive industrial scenarios’ is supported by the Carl-Zeiss-Stiftung. The authors would like to thank the funding agency for the financial support and the continuous assistance during the project runtime.

Declaration of Competing Interest

None.

References

Baxter, J., 1995. Learning internal representations. Proceedings of the Eighth Annual Conference on Computational Learning Theory, pp. 311–320.
Bejlegaard, M., Brunoe, T.D., Nielsen, K., 2018. A changeable jig-less welding cell for subassembly of construction machinery. IFIP International Conference on Advances in Production Management Systems. Springer, pp. 305–311.
Breiman, L., 2001. Random forests. Mach. Learn. 45 (1), 5–32.
Chen, L., Zhou, L., Tang, C., Huang, W., Wang, C., Hu, X., Wang, J., Yan, F., Wang, X., Jiang, Z., et al., 2014. Study of laser butt welding of SUS301l stainless steel and welding joint analysis. Int. J. Adv. Manuf.Technol. 73 (9), 1695–1704.
Cho, K., Van Merriënboer, B., Gulcehre, C., Bahdanau, D., Bougares, F., Schwenk, H., Bengio, Y., 2014. Learning phrase representations using RNN encoder-decoder for statistical machine translation. arXiv preprint arXiv:1406.1078.
Dal, M., Fabbro, R., 2016. An overview of the state of art in laser welding simulation. Opt. Laser Technol. 78, 2–14.
Danielewski, H., Skrzypczyk, A., 2020. Steel sheets laser lap joint welding-process analysis. Materials 13 (10), 2258.
Dennis Jr., J.E., Welsch, R.E., 1978. Techniques for nonlinear least squares and robust regression. Commun. Stat.-Simul.Comput. 7 (4), 345–359.
He, K., Zhang, X., Ren, S., Sun, J., 2016. Deep residual learning for image recognition. Proceedings of the IEEE Conference on Computer Vision and Pattern Recognition, pp. 770–778.
Heller, K., Kessler, S., Dorsch, F., Berger, P., Graf, T., 2015. Robust æfalse friendg detection via thermographic imaging. Proceedings of Lasers in Manufacturing Conference (LIM).
Hochreiter, S., Schmidhuber, J., 1997. Long short-term memory. Neural Comput. 9 (8), 1735–1780.
Högel, R., 2017. Next generation of jigless robot welding: industry 4.0 conformant welding cell for batch sizes down to 1. Laser Technik J. 14 (4), 39–41.
Hsu, R., Engler, A., Heinemann, S., 1998. The gap bridging capability in laser tailored blank welding. International Congress on Applications of Lasers & Electro-Optics, Vol. 1998. Laser Institute of America, pp. F224–F231.
Ioffe, S., Szegedy, C., 2015. Batch normalization: accelerating deep network training by reducing internal covariate shift. International Conference on Machine Learning. PMLR, pp. 448–456.
Kampker, A., Bergweiler, G., Hansen, J.O., Borbola, W.J., 2017. Jigless laser welding in the car body production. ATZ Worldwide 119 (2), 72–75.
LeCun, Y., Haffner, P., Bottou, L., Bengio, Y., 1999. Object recognition with gradient-based learning. Shape, Contour and Grouping in Computer Vision. Springer, pp. 319–345.
Mrna, L., Hornik, P., 2016. Autocorrelation function for monitoring the gap between the steel plates during laser welding. Phys. Procedia 83, 1223–1232.
Nagel, F., Simon, F., Hildebrand, J., Bergmann, J., 2017. Optimisation strategy for the laser beam welding of high-alloyed steels. Welding Cutting 16 (4), 257.
Nilsen, M., 2017. Optical detection of joint position in zero gap laser beam welding. University West. Ph.D. thesis.
Otsu, N., 1979. A threshold selection method from gray-level histograms. IEEE Trans. Syst. Man Cybern. 9 (1), 62–66.
Radaj, D., 1988. Wärmewirkung des Schweißens. Buch, 265 Seiten. Springer Verlag (Berlin).ISBN: 978-3-540-18695-3
Rumelhart, D.E., Hinton, G.E., Williams, R.J., 1985. Learning Internal Representations by Error Propagation. Technical Report. California Univ San Diego La Jolla Inst for Cognitive Science.
Schenk, T., 2011. Modelling of welding distortion; the influence of clamping and sequencing.
Schmidt, L., Junger, C., Schricker, K., Bergmann, J.P., Notni, G., 2021. Echtzeitfähige Ansätze zum Monitoring der dehnungsfeldbasierten Spaltentstehung und resultierender Nahtqualität beim Laserstrahlschweißen. Innovative Verfahren der Lasermaterialbearbeitung, manuscript ed. Düsseldorf : DVS Media GmbH, 2021.
Seang, C., David, A., Ragneau, E., 2013. Nd: Yag laser welding of sheet metal assembly: transformation induced volume strain affect on elastoplastic model. Phys. Procedia 41, 448–459.
Shi, J., Chang, Y., Xu, C., Khan, F., Chen, G., Li, C., 2020. Real-time leak detection using an infrared camera and faster R-CNN technique. Comput. Chem. Eng. 135, 106780.
Simon, F.B., Nagel, F., Hildebrand, J., Bergmann, J.-P., 2013. Optimization strategies for welding high-alloy steel sheets. Schweißen und Wärmebehandlung, vol. 189.
Srajbr, C., Tanasie, G., Dilger, K., BÖhm, S., 2011. Active thermography for quality assurance of joints in automobile manufacturing. Welding World 55 (7), 90–97.
Srivastava, N., Hinton, G., Krizhevsky, A., Sutskever, I., Salakhutdinov, R., 2014. Dropout: a simple way to prevent neural networks from overfitting. J. Mach. Learn. Res. 15 (1), 1929–1958.
Vater, J., Kirschning, M., Knoll, A., 2020. Closing the loop: real-time error detection and correction in automotive production using edge-/cloud-architecture and a CNN. 2020 International Conference on Omni-layer Intelligent Systems (COINS). IEEE, pp. 1–7.